The role of small-scale sediment topography for oxygen flux across the diffusive boundary layer

Hans Røy,[1] *Markus Hüttel, and Bo Barker Jørgensen*

Max-Planck-Institute for Marine Microbiology, Celsiusstrasse 1, D-28359 Bremen, Germany

Abstract

At the scale of centimeters or millimeters, marine sediment surfaces are sculptured into complex three-dimensional landscapes. A detailed study of fluxes through the diffusive boundary layer (DBL) therefore requires concurrent information on the surface structure. Using natural sediment in a laboratory flume, we investigated the impact of small-scale sediment topography on diffusive oxygen flux through the DBL. Topographic maps of the sediment surface with 0.1 mm horizontal resolution were acquired with a custom-made optical technique, and immediately afterward the oxygen diffusion field across the sediment–water interface was measured with microsensors in known orientation within the described topography. A method was developed to calculate the three-dimensional diffusive flux through the DBL, based on the combination of vertical O_2 microprofiles and the high-resolution topographic data. Even though the sediment surface investigated was elaborately sculptured by fauna, the combined influence of increased surface area and horizontal concentration gradients within the DBL induced less than 10% difference between one-dimensional and three-dimensional diffusive flux calculations. The relatively low impact of surface topography is explained by the geometry of the diffusion field, as well as effects of the rapid diffusion of O_2 at small scales.

The diffusive boundary layer (DBL) is the thin film of water covering fine-grained sediments, through which molecular diffusion is the dominant transport mechanism for dissolved material. Viscous forces reduce turbulent mixing in the lowest part of the benthic boundary layer. At a distance of a few tenths of a millimeter from the sediment surface, turbulent mixing becomes insignificant for the transport of dissolved substances relative to molecular diffusion (Boudreau and Jørgensen 2001). The lowest part of the DBL is therefore characterized by linear concentration profiles.

As with the velocity boundary layer, the upper limit of the DBL is not well defined. Here, the concentrations of dissolved substances approach the free-stream concentration asymptotically. Jørgensen and Revsbech (1985) introduced the effective DBL (Z_δ) as a practical definition of the DBL thickness. According to this definition, the upper DBL limit is found by extrapolating the gradient at the sediment surface to the free-stream concentration. Defined this way, the effective DBL is functionally equal to the actual DBL with respect to transport via molecular diffusion across the layer.

Although the thickness of the DBL in marine environments is only 0.2–1.2 mm (Jørgensen 2001), the DBL can play an important role for reactions for which the rate or

spatial distribution is controlled by transport resistance (Boudreau and Guinasso 1982). Examples are dissolution or precipitation reactions such as the accretion of ferromanganese nodules (Boudreau 1988) or the rapid exchange of nutrients and gases between surface sediments and water column (Jørgensen and Revsbech 1985; Blackburn et al. 1994; Canfield and Teske 1996).

Oxygen plays a key role for the respiration of benthic microbial communities. As oxygen is relatively easy to measure, it has been the preferred model substance for diffusive boundary layer studies. Owing to its low solubility in seawater and high rate of consumption, oxygen generally penetrates only a few millimeters into fine-grained coastal sediments (Revsbech et al. 1979; Cai and Sayles 1996). Therefore, the DBL can constitute a significant transport resistance for oxygen flux between water and these sediments. With microsensors, direct measurements of oxygen concentration gradients in the DBL are possible. The diffusive flux (J) through the DBL and across the sediment–water interface can be calculated using Fick's first law of diffusion:

$$J = -DdC/dz \qquad (1)$$

where D is the molecular diffusion coefficient and dC/dz the vertical concentration gradient. Such calculations of diffusive fluxes based on measured microprofiles of gases and ions are common in aquatic science (e.g., Jørgensen and Revsbech 1985; Rasmussen and Jørgensen 1992; Steinberger and Hondzo 1999; Boudreau 2001).

Our current conceptual understanding of the DBL, as well as the application of the simple Fick's first law of diffusion, treats the sediment–water interface as an infinite flat plane crossed by one-dimensional chemical gradients. However, sediment surfaces are sculptured into elaborate landscapes when viewed at the scale of the DBL (Paul et al. 1978; Swift et al. 1985; Briggs 1989; Gundersen and Jørgensen 1990; Jørgensen and Des Marais 1990; Wheatcroft 1994; Fenchel 1996; Ziebis et al. 1996*a,b*), and this surface topography also

affects the structure of the DBL. For example, on the upstream side of obstacles the DBL is compressed, whereas on the lee side it is expanded. Surface structures with a characteristic dimension smaller than half the thickness of the DBL, however, are not reflected in the oxygen gradients within the DBL (Jørgensen and Des Marais 1990).

When compact topographical structures protrude through the viscous sublayer, they induce turbulence. Thus the interaction between topography and flow influences the thickness of the DBL, not only locally but also far downstream of the structures themselves (Boudreau and Guinasso 1982; Weissburg and Zimmer-Faust 1994). The hydrodynamic mechanisms that regulate the thickness of the DBL are, however, out of the scope of this study.

Owing to surface topography, horizontal as well as vertical gradients are present in the DBL. In addition, the effective exchange area is larger than the projected horizontal area, which suggests that the microbial community can exchange solutes with the overlying water more effectively than predicted from one-dimensional models and measurements.

Two-dimensional O_2 distributions at the sediment–water interface have been presented from decaying detritus (Jørgensen and Revsbech 1983), mats of colorless sulfur bacteria (Jørgensen and Revsbech 1983; Fenchel and Bernard 1995), and biofilms (de Beer et al. 1994; de Beer and Stoodley 1995). Across this range of communities, with laminar to turbulent flows, isolines of oxygen concentration are smooth lines loosely following the relief of the sediment–water interface. Even a sediment relief elaborately structured by polychaete tubes (Jørgensen and Revsbech 1985) shows no large deviation from this picture. Electrode-independent methods with a resolution better than 30 μm show the same smoothed out isolines compared to the sediment surface (Glud et al. 1996). The reason for the smoothness is that, at the small scale, molecular diffusion levels out any heterogeneity in solute distribution that is not maintained by effective sinks and sources. It is the same diffusion effect that causes microprofiles to be smooth and continuous in one-dimensional representations. Irregular microprofiles are mostly caused by temporal variation or instrument noise. Isolines contain important information about diffusive fluxes. Since concentrations are constant along these lines, no net diffusion occurs along them and the direction of diffusive transport is at right angles to the isolines. The slope of an isoline touching the sediment surface at a specific point will, therefore, define the angle at which net diffusion across the sediment–water interface occurs at that point.

For most surfaces, the isolines clearly do not describe an infinite flat plane. To account for complex three-dimensional diffusion in biofilms, de Beer and Stoodley (1995) analyzed horizontal gradients around vertical surfaces of cell clusters, as well as vertical gradients across horizontal surfaces. By estimating the coverage of the various surface structures with a confocal scanning laser microscope, they calculated diffusive fluxes taking into account all spatial dimensions. Given that the DBL was kept thin (high flow velocity) relative to the biofilm landscape of ~300-μm diameter cell clusters and 100-μm wide voids, the total mass transport exceeded the calculated one-dimensional flux by 100–150%.

During less extreme flows, however, the topographic effect was almost completely smoothed out.

Jørgensen and Des Marais (1990) applied a different approach to calculate the flux across a mapped complex topography: By assuming that the path of diffusion was normal to the sediment surface and that the exchange area was defined by the upper DBL limit, they calculated a correction factor for the average vertical flux that accounted for both underestimated gradients and underestimated exchange area. By using their so-called double cosine correction on the oxygen flux across the sediment–water interface of a hypersaline microbial mat, they calculated that surface topography increased the flux by 49% relative to a one-dimensional diffusive flux calculated from the vertical oxygen microgradients.

The aim of the present study was to analyze the relation between surface roughness and three-dimensional diffusive fluxes through the DBL of marine sediments. For this purpose, a laser-based light striper method was developed for mapping surface topography with a horizontal resolution better than 100 μm. The relationship between diffusive flux and topography then was investigated by acquiring spatially structured microsensor data within the mapped topography. As an alternative to sampling a natural location, a sediment block was brought to the laboratory and allowed to develop a stable community. With respect to the relationship between diffusive flux and topography, the artificial community was considered representative for coastal sediments, where surface structures, solute fluxes, and chemical zonations are governed by microbial metabolism, redox reactions, diffusion, and bioturbation.

Materials and methods

Flume and sediment—The experimental work was conducted under unidirectional flow in a laboratory flume 300 cm long, 30 cm wide, and 25 cm high. Subtracting a total of 40 cm from the channel length for flow conditioning, the flume accommodates a 260 cm free-flow section. Undisturbed layers of silty surface sediment (60 cm long, 30 cm wide, and 5 cm thick) were collected at low tide from an intertidal mudflat of the German Wadden Sea. These sediment blocks were placed with intact stratification in the flume, covering the entire length of the free-flow section. The flume was then filled with filtered North Sea water to produce a water depth of 10 cm above the sediment.

The developing flow along the free-flow section lead to different structure of the DBL in different parts of the flume. Most notably, O_2 profiles measured only a few centimeters downstream from the inflow show a much more abrupt transition from free-flow O_2 concentration to the linear gradient in the DBL than what is observed from in situ profiles (e.g., Gundersen and Jørgensen 1990). Also the temporal dynamics of the DBL within the flume change with the developing flow structure. Dependencies of concentration fluctuations on flow parameters have been described from other experimental systems (Gundersen and Jørgensen 1990; Jørgensen and Des Marais 1990; Güss 1998), but the mechanisms behind are poorly understood. With the flume dimensions and

sediment roughness used in this study, an increasing insta-bility of the DBL was observed with increasing distance from the water inlet. A similar effect was observed when the flow velocity was increased, which is in contrast to the observations of Gundersen and Jørgensen (1990). This dis-crepancy is most likely due to the larger size of the flow channel used in this study.

In order to maintain a stable sediment respiration, tem-perature was kept constant at 19°C and organic material was supplied to the sediment surface in the form of homogenized algae once every month. Accumulation of nutrients in the flume was prevented by occasionally exchanging the entire water volume of 91 liters. Before the experiments were start-ed, the sediment had been maintained in the laboratory for 2 yr.

At the time of the experiments, the infauna was dominated by oligochaetes of the Tubificidae family, which did not pro-duce visible burrows. The worms deposited black fecal ma-terial on the surface in small circular mounds. Within 1 h the mounds collapsed, leaving slightly raised black spots of 1–2 mm diameter. After another 4–5 h the spots gradually vanished, unless the worms supplied new material. Repeated defecation at the same positions formed sediment mounds of up to 5 mm in diameter, similar in color to the undisturbed surfaces. The abundance of oligochaetes was more than 5,000 per m^2 and, consequently, their mounds were domi-nating features on the sediment surface.

Another conspicuous feature was fecal mounds produced by the polychaete *Heteromastus filiformis*. These mounds were 5 to 10 mm high and occurred at a density of 110 m^{-2}. These mounds were cone shaped and consisted of ~0.5 mm long, uniformly egg-shaped pellets.

The macrofauna included a few juvenile individuals of the common shrimp, *Crangon crangon*. The life expectancy of these crustaceans was 6 to 12 months, and they were the only animals in the flume restocked. The physical activity of the shrimps had a strong influence on the surface struc-ture, as the sediment surface without physical disturbance would completely turn into overlapping fecal mounds. In-spection of the sediment with a dissection microscope re-vealed that the surface microstructure consisted entirely of fecal material in different stages of disintegration. The sub-surface sediment, however, did not appear to be formed by discrete pellets.

Median grain size of the sediment was 6.3 μm. Porosity, as determined by drying samples at 60°C until constant weight, was 77% in the upper 15 mm (SE 2.5, $n = 5$). Permeability in the top 18 mm was 1.52×10^{-13} m^2 (SE 2.85×10^{-14} m^2, $n = 3$), measured with a constant head of 500 Pa (Klute and Dirksen 1986). The organic carbon con-tent was 2.9% dry weight (SE 0.2, $n = 10$), determined with a carbon-nitrogen-sulfur (CNS) analyzer.

Topographic mapping—For optical measurements of to-pography, a laser line was projected vertically down on the sediment surface from a diode laser (Lasiris LAS-670-5 laser with LAS-1 line-20° TS line generator). A glass plate sus-pended in the air–water interface assured that refraction was constant and well defined (Fig. 1). The cross-section of the 0.2-mm wide laser line had a Gaussian intensity distribution.

Along the central 55 mm of the line used for measurements, light intensity and line width varied insignificantly. An im-age of the projected laser line was recorded by a digital camera (1,280 × 1,024 pixel PCO SensiCam with a 35-mm objective). The camera was pointed at the laser line at an angle of 45°. Owing to refraction in the air–glass–water in-terface, the resulting angle between the camera axis and ver-tical was approximately 30°.

For each vertical column of pixels in the digital image, the position of the laser line was determined. Subpixel ac-curacy was achieved by the use of a three point estimator and the known Gaussian intensity distribution across the line (Raffel et al. 1998). In this way, the image was transformed to an array of surface elevations, expressed in pixel coor-dinates (Fig. 2A).

To calculate the scale between the pixel coordinates and real distances (Fig. 2B), a 1-mm line grid was imaged in the plane of the laser sheet. Separate vertical scales for each pixel column were found by linear regression on the known calibration points. Given a distance of 300 mm between camera and the 60 mm wide projected laser line, the per-spective distortion induced by the central projection of the imaging system was insignificant. Therefore, the vertical scale did not vary measurably within the images, and the linear regressions consistently gave r^2 values better than 99.9%. The mean scale of all 1,280 pixel columns was used to transform the vertical pixel scale into millimeters.

Likewise, the horizontal scale was determined for each horizontal row of pixels in the image. Owing to the 60-degree tilt of the image plane of the camera relative to the laser beam, the horizontal scale was a function of the vertical position in the image. Therefore, the scaling factor from the pixel row best representing the average position of the laser line was used for horizontal calibration. Within the band of pixel rows ever containing the sediment surface, the differ-ence in scale between the highest elevations and the deepest depressions was less than 1.4%.

To extend the data to three dimensions, the laser-camera assembly was moved horizontally in 100-μm steps perpen-dicular to the laser line. Assembling data from 601 images, the sediment area covered in each mapping procedure was 55 × 60 mm (Fig. 2C). The horizontal resolution was 100 μm in the direction of translation and approximately 50 μm along the laser line. As data points were evenly distributed along both horizontal axes, the data could be written into the matrix format of the software package Surfer 6 (Golden Inc.) without transformation.

In general, more than 99% of the measured points had an elevation within 100 μm of the average elevation of their immediate neighbors. However, owing to occasional oligo-chaete worms or plant fibers protruding from the sediment, ~1% were found as isolated points several millimeters up into the water column. Such outlying points, which were not part of the sediment surface, were removed from the dataset and a new point was interpolated.

On topographic slopes steeper than 60° and facing away from the camera, the sediment would obstruct the camera's view of the laser line. The mapping algorithm finds the po-sition of the laser line based on the position of the maximum light intensity within each column of pixels. It will, there-
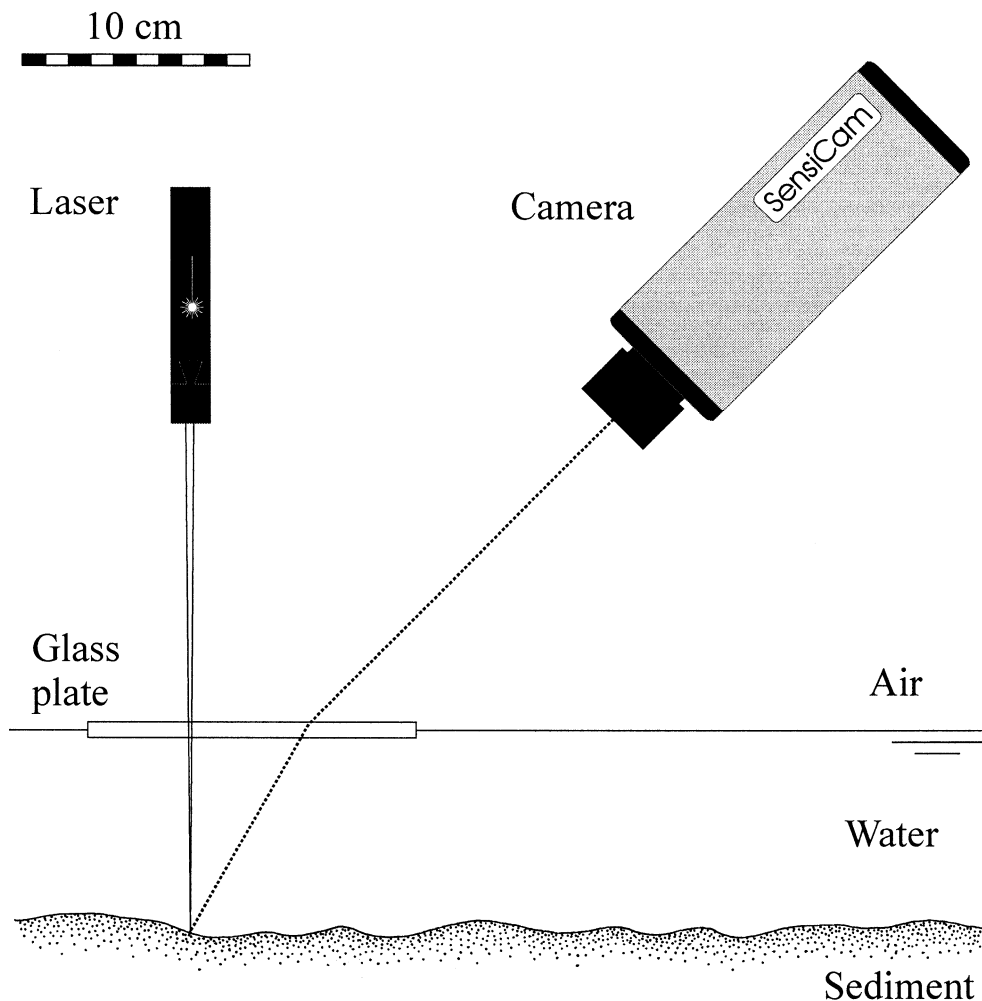
Fig. 1.   Setup used to measure sediment topography. The digital camera, the laser, and the glass plate were combined in one rigid mechanical unit.

fore, propose a position even when the laser line is not visible to the camera. In these cases the maximum intensity found is low compared to what is found when the laser line is visible and it is easily identified as invalid. Such steep surface elements were rare and covered ≪1% of the surfaces measured.

Image recording and motion control, as well as data extraction and processing, were performed by routines written in Labview with IMAQ vision extension (National Instruments). The routines for data extraction are available as MS Windows executable files from the first author.

Microsensor analysis—In order to assess spatial oxygen variability, temporal concentration variation had to be min-imized. As a compromise between downstream flow development and DBL stability, the microelectrode data presented were recorded at the flume centerline 50-cm downstream from the leading edge of the sediment block. The O_2 sensors used were Clarke type microelectrodes with internal reference and guard cathode (Revsbech 1989). Tip diameters were 15 μm, stirring sensitivity less than 1%, and response time about 1 s. The electrodes were calibrated between the O_2 concentration in the mixed water column determined by Winkler titration and anoxic sediment, assuming a linear current response. The electrode signal was recorded on an IBM compatible PC using a LAB-PC 1200 AI analog-to-digital converter (National Instruments). The microsensors were positioned using a computer-controlled motorized translation

$\rightarrow$

Fig. 2.   (A) Digital image of the intersection between a laser sheet and the sediment surface, generated with the setup shown in Fig 1. (B) The topographic profile derived from (A) consisting of 1,088 data points, one for each pixel column in the digital image. (C) Topography of a 60 × 55 mm sediment surface area depicted as a computer generated shaded relief. The data were assembled from the topographic profile shown in (B), together with another 600 similar profiles. The direction of scanning was from left to right. A more detailed map of the framed area can be seen in Fig. 6.

A: Digital image

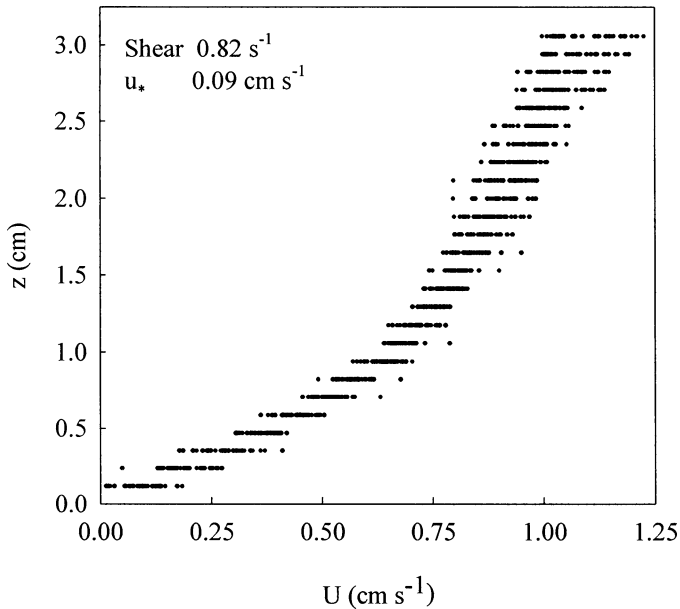B: Derived profile

C: Assembled topography
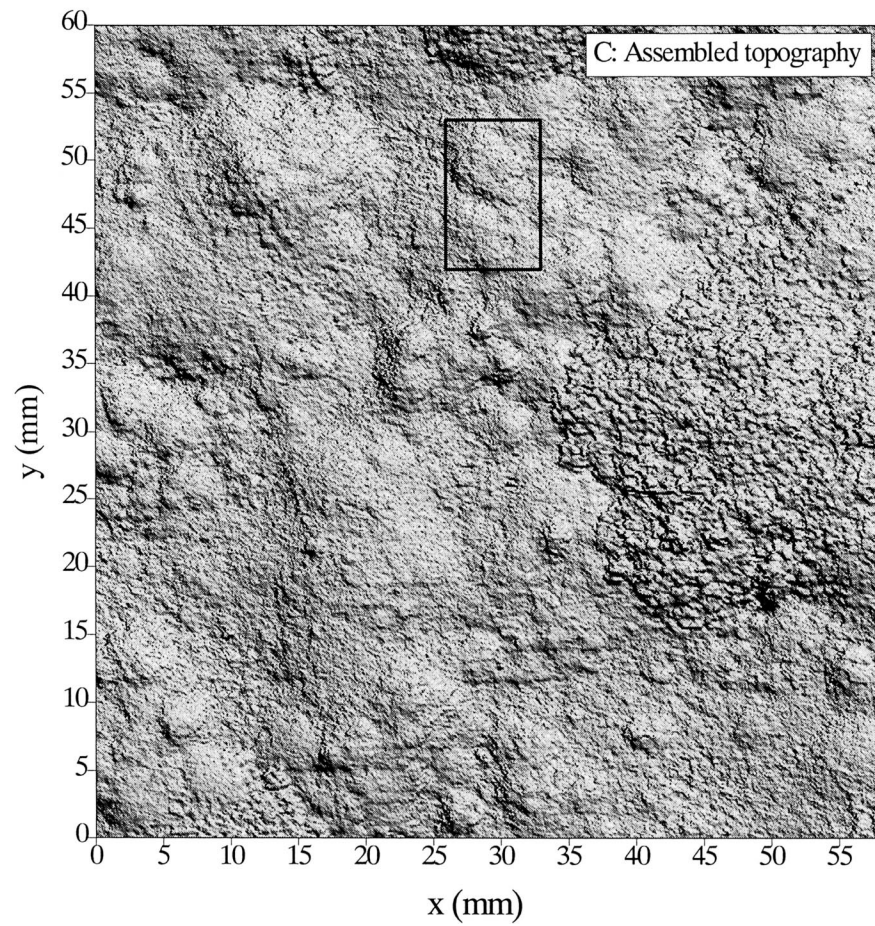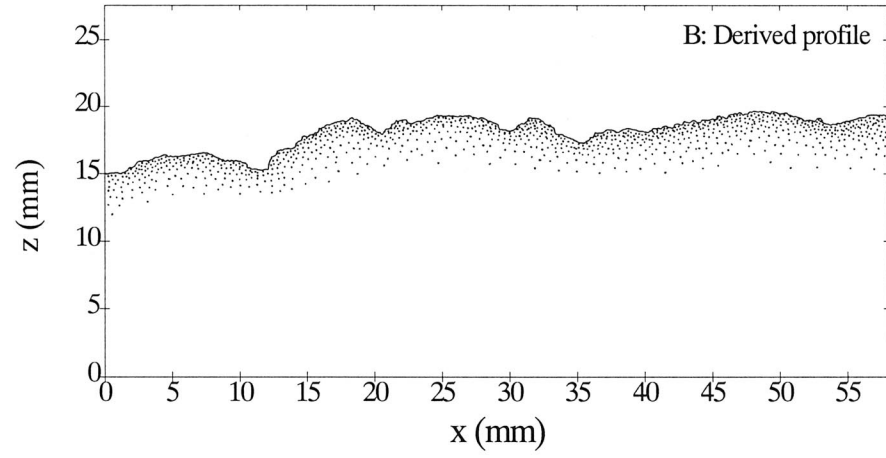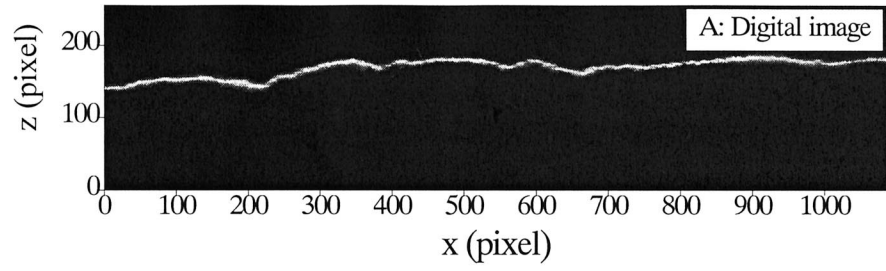
Fig. 3. Vertical flow velocity profile above the sediment surface measured with digital particle image velocimetry (PIV). The points are single measurements. The position of the sediment surface was determined from the images used for the PIV. The shear is found by linear regression of the lowest 10 mm of the profile. Shear stress (τ_b) is calculated as shear multiplied with dynamic viscosity (ν) at the appropriate temperature and salinity. Shear velocity (u_*) is calculated according to the equation $u_* = (\tau_b/\text{density})^{1/2}$. For a description of PIV, see Raffel et al. (1998).

table (Physik Instrumente M-150.20) for each of the three axes. By recording evenly spaced vertical microprofiles, two-dimensional grids of O_2 distributions were acquired. Horizontal and vertical resolutions were 100 μm.

Optical fibers with light-scattering titanium dioxide coated tips were introduced through silicone-rubber ports built into the flume bottom. When placed exactly at the sediment surface and illuminated from below, the tips provided luminescent fix points that were used to align microsensor and laser scanning measurements horizontally. Vertical alignment between oxygen microprofiles and topographic maps were based on the change in oxygen gradient at the sediment–water interface (Rasmussen and Jørgensen 1992). The use of aligned profiles assured ample numbers of profiles with sufficiently distinct changes in gradients to make an accurate determination with this technique.

Results

Flow structure—Figure 3 shows the vertical velocity profile in the region of the flume where microsensors were deployed. Shear velocity (u_*), determined from the velocity gradient in the linear part of the profile, was 0.09 cm s^{-1}. Assuming the free-stream velocity above the logarithmic layer to be approximately 20 u_* (Denny 1993), the corresponding free-stream velocity would be 1.8 cm s^{-1}. This flow velocity is in the low range for coastal marine environments. But a well-developed transition between DBL and turbulent mixed water column showed that the conditions

were still far from stagnant (Fig. 4B). Shape and gradient of our microprofiles compared well with those measured in similar sediments in the field (e.g., Gundersen and Jørgensen 1990). According to our experience, a shorter free-flow distance would have produced a more stable DBL resulting in smoother isolines, but would have compromised the desire for a realistic microprofile shape.

Topography and microsensor measurements—Selected areas of sediment surface were mapped twice with the described line striping method (Fig. 2C). Between the scannings, transects of vertical O_2 distribution through the sediment–water interface were recorded within the mapped areas (Fig. 4A). The 3- to 5-mm long oxygen transects were placed so that the macroscopic topography was symmetrical around the transect. The oxygen gradient perpendicular to the plane could therefore be assumed to be minimal. Owing to the long measuring procedure of several hours per transect, the dense population of oligochaetes would occasionally modify the topography within the areas where O_2 microprofiles were being recorded. In such instances, the topographic data as well as the [O_2] transect were discarded. Flat areas not recently disturbed by macrofauna had a uniform O_2 penetration of about 2.9 mm, while the disturbed areas displayed considerable variation.

Single-point three-dimensional flux calculations—From the two-dimensional O_2 data, isolated vertical microprofiles can be extracted (Fig. 4B). The gradient (dC/dz), describing the vertical diffusive flux (J_z) down to the sediment surface, can be found by linear regression of the data in the lowest 300 μm of the DBL. Similarly, the horizontal gradient at the same point of the surface can be found by selecting O_2 data from the same depth of neighboring profiles. Analogous to the vertical flux, the horizontal flux (J_x) is calculated based on the gradient from the horizontal row of points stretching from the sediment surface into the water column (Fig. 4C).

To calculate the magnitude and direction of the resulting diffusive flux, we consider J_x and J_z as vectors (Fig. 4D). If there is no horizontal gradient perpendicular to the measured vertical plane, the measured vertical and horizontal flux vectors can be used to calculate the resultant vector, J_n. The magnitude of J_n and the angle (α) between J_n and vertical are found by simple trigonometry:

$$J_n = (J_x^2 + J_z^2)^{1/2} \tag{2}$$

$$\cos \alpha = J_z/J_n \tag{3}$$

Rearranging Eq. 3, we get an expression for J_n as function of the angle (α) and the vertical flux:

$$J_n = J_z \times 1/\cos \alpha \tag{4}$$

A flux is defined as the transport per unit area and time. The exchange area (A') should be measured perpendicular to the direction of diffusion (Fig. 4D). Similar to the relation between J_n and J_z, the relation between A' and the projected horizontal area (A) can be described by the angle (α) between horizontal and A':
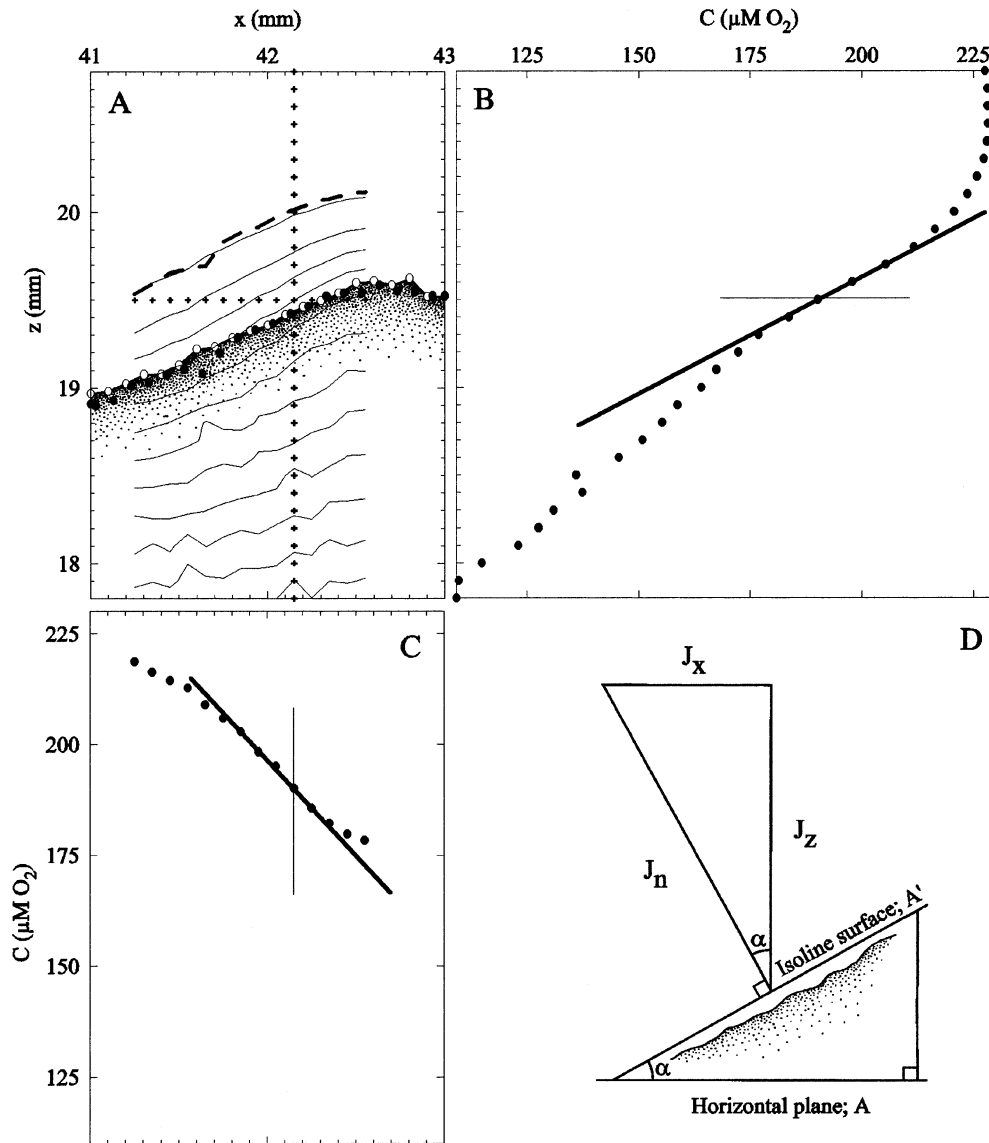
$$A'/A = 1/\cos \alpha \tag{5}$$

Fig. 4. (A) Vertical section of the sediment–water interface. The circles indicate points determined on the sediment surface by two successive scanning procedures. Filled circles are from the first pass, while open circles are from the second. In the vertical plane, the O_2 concentration was measured with 100 by 100-μm grid spacing. Isolines of equal O_2 concentration are shown as thin black lines, while the upper limit of the effective DBL (Jørgensen and Revsbech 1985) is drawn as a thicker dashed line. The vertical column of crosses indicates the position where the O_2 profile shown in panel (B) was recorded. Likewise, the horizontal row of crosses indicates where the profile shown in panel (C) was recorded. (B) Vertical O_2 microprofile extracted from the two-dimensional distribution in (A). The vertical flux (J_z) can be calculated from the slope of the profile (thick line) above the sediment surface. (C) Horizontal O_2 microprofile extracted from the two-dimensional O_2 distribution in panel (A). Analogous to the vertical flux, the horizontal flux (J_x) can be calculated from the slope of the profile (thick line) leading from the water column toward the sediment surface. (D) Geometric representation of the two-dimensional flux calculation (*see text for details*).

The plane defined by A' in Fig. 4D is perpendicular to J_n. The concentration gradient along this plane is therefore zero, i.e., this is locally an isoline of constant concentration. Accordingly, the local magnitude of $1/\cos \alpha$ can be calculated from the area of the isoplanes, where these intersect the sediment surface and the projected horizontal area underneath them.

Figure 4D shows that the α used for exchange-area calculation and α used to calculate J_n from J_z are identical. The parameter $1/\cos \alpha$ is the relation between total exchange area and projected horizontal area as well as the ratio J_n/J_z. It is generally convenient to express a measured flux between water column and sediment based on the projected horizontal area rather than based on the actual exchange area. Fol-
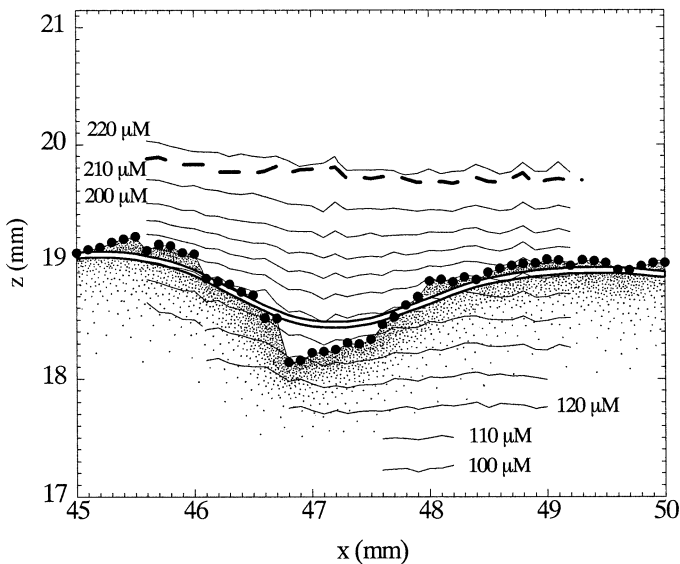
Fig. 5. O$_2$ distribution at sediment surface topography. The O$_2$ isolines are represented by thin lines, while the upper limit of the effective DBL (Jørgensen and Revsbech 1985) is drawn as a thicker dashed line. Filled circles are points determined as the sediment surface by optical line striping. By smoothing the sediment surface with a matrix with the same size as the thickness of the DBL (1.4 mm), a surface that is nearly parallel to the isolines is generated (double line). Not every profile has been extended to the full oxygen penetration depth. The areas where isolines are seen represent the areas where data are present in full resolution.

lowing the nomenclature of Jørgensen and des Marais (1990), we will call this flux J'. Combining Eqs. 4 and 5, a relation between J', J_z, and α can be written

$$J' = J_z \times (1/\cos \alpha)^2 \qquad (6)$$

Area-based three-dimensional flux calculations—When dealing with areas rather than single points, the relationship between A' and A will be more readily available than the distribution of α. As we will focus on the difference between J' and J, we rearrange Eq. 6 and base it on A'/A to get the expression

$$J'/J_z = (A'/A)^2 \qquad (7)$$

To apply Eq. 7 directly, we would have to map an isoplane over extensive areas. For bioturbated sediments, the required area coverage is not possible via conventional single-point microsensor measurements. Alternatively, equivalent information can be found from high-resolution topographic data. As seen in Fig. 5, the O$_2$ isolines do not follow the smallest details of the sediment topography. They rather resemble a smoothed sediment surface, lacking features that are much smaller than the thickness of the DBL. The same smoothing effect can be imposed mathematically on the measured sediment topography by replacing each measured height with the average of all heights within a distance corresponding to the thickness of the effective DBL (Z_δ). By smoothing that way, a virtual sediment surface that is nearly parallel to the isolines can be obtained (Figs. 5 and 6). By using A'/A from

these approximated isolines, the ratio between vertical and horizontal fluxes can be calculated for the entire topographical map. By varying the size of the smoothing kernel, different thicknesses of DBLs can be simulated independent of the actual DBL thickness during measurements. In addition to the scannings made in connection with the O$_2$ measurements, five random areas along the centerline of the flume were mapped. For each map, J'/J_z was estimated from topography based on a range of smoothing-kernel sizes (Fig. 7). The interpolated line of J'/J_z plotted against the applied smoothing-kernel size shows the dependency of J'/J_z on DBL thickness and will be characteristic for a given sediment. From the vertical axis of Fig. 7, we can now read the factor J'/J_z for a range of DBL thicknesses. This factor must be multiplied to a flux calculated from a vertical microprofile to get the total diffusive flux (J').

Vertical DBL thicknesses in the flume, measured from above, ranged between 0.4 and 1.4 mm with an estimated average of 0.6 mm. When a 0.6 mm smoothing kernel is used for the estimation of J'/J_z, a 10% difference is found between one-dimensional vertical flux calculation and the calculation taking topography into account ($J'/J_z = 1.1$ in Fig. 7).

The DBL thicknesses quoted here were, however, measured from above and thereby underestimated due to compression of the DBL during measurement (Glud et al. 1994). Lorenzen et al. (1995) described the effect of the DBL compression as equivalent to an increase in flow velocity. Accordingly, the thinning of the DBL should cause the O$_2$ isolines to follow the sediment surface more closely than in the absence of the sensor (Jørgensen and Des Marais 1990; Gundersen and Jørgensen 1990; de Beer et al. 1996). A topography smoothing matrix that successfully reproduces isolines measured from above will, therefore, leave topographic features that would be smoothed out by the thicker DBL when the sensor is not present and A'/A will be overestimated. The 10% difference between J_z and J' calculated from a 0.6 mm matrix is thereby a maximum estimate.

Discussion

Jørgensen and Des Marais revisited—In order to compare our method and results to those of Jørgensen and Des Marais (1990), we recalculated their raw data. As these authors acquired both oxygen isolines and topography, a comparison between cosine correction based on smoothed topography and cosine correction based directly on isolines can be made: by smoothing the topographic data with a range of kernel sizes, estimates of J'/J_z for different thicknesses of DBLs were calculated. Figure 7 shows that such a calculation would relate the mean Z_δ of 0.52 mm that was measured by these authors to a correction factor slightly above 1.4. Jørgensen and Des Marais (1990) defined the upper DBL limit as the 90% O$_2$ saturation isoplane and reported A'/A for this isoplane to be 1.14. Following Eq. 7, J'/J_z based on the isoplane alone is 1.3.

Although O$_2$ isolines are mostly parallel down through the DBL, they are somewhat smoother in the upper part of the DBL than at the sediment–water interface. The J'/J_z of 1.30
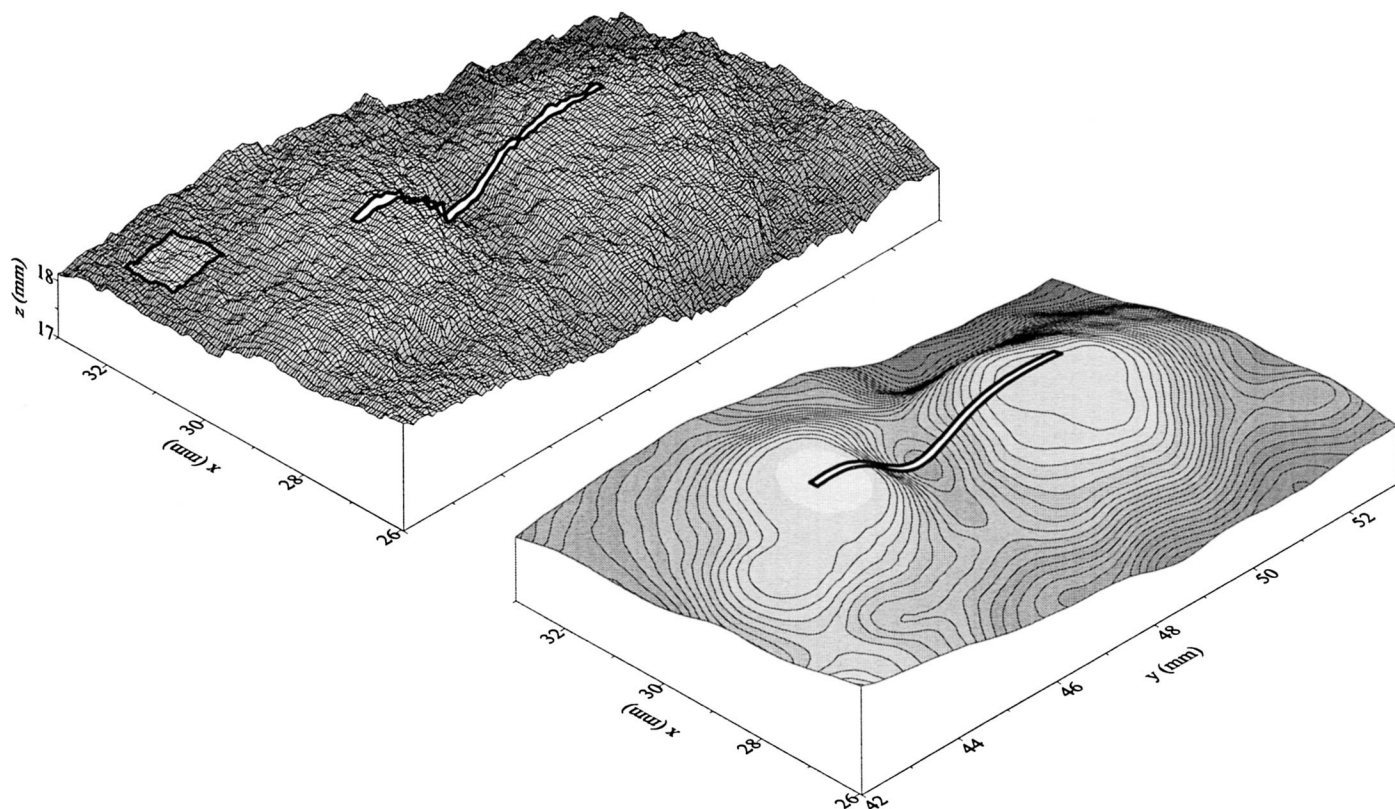
Fig. 6. Small section of a topographic map before and after data smoothing. The square insert in the nonsmoothed surface indicates the size of the smoothing matrix. The smooth surface mimics the distribution of an arbitrary O_2 isoline and can be used to calculate A'/A and thereby J'/J_z (*see text for details*). The cutout was taken from the map shown in Fig. 3C. The double line marks the position where the transect shown in Fig. 5 was recorded.

calculated based on the 90% isoplane should, therefore, be considered a minimum estimate. On the contrary, the J'/J_z of 1.49 reported in the original manuscript may be considered as an overestimation, since their assumption that the flux is normal to the sediment topography is incompatible with the discrepancy between sediment surface and isoline topography. Apart from the fact that the correction method based on smoothed topography gives a value between minimum and maximum estimate, one should note that topographic data are not included in the correction calculated to be 1.3, and chemical data are not included in the calculation of the factor 1.4.

The different dependencies of J'/J_z on DBL thickness between the data from the current study and the data from Jørgensen and Des Marais (1990) are linked to differences in surface morphology. The surface of the microbial mat was structured by tufts and clusters of cyanobacteria and diatoms, with dimensions of the same scale as the DBL. The degree of smoothing imposed by the DBL is therefore critical. In the case of the bioturbated sediment, the surface roughness was dominated by structures that were either below or above the range of potential DBL thicknesses. The DBL thickness, and thereby flow velocity, was in the latter case much less critical for the influence of topography on the ratio J'/J_z.

A similarly direct comparison to method and results of de Beer and Stoodley (1995) is not possible, since topographical maps were not acquired. However, these authors also observed that the effect of 100–300-μm scale topography was dependent on the DBL thickness: with a $<$50-μm thick DBL the isolines and DBL would follow the complex surface structure and a large topographic effect could be observed, whereas a 100–200-μm thick DBL excluded topographic effects. A similar result would have been produced from a smoothed topography approach, because a smoothing kernel of 50-μm square would change the depicted topography only slightly, while a 150-μm kernel would effectively fill in the 100-μm voids.

Applicability of the method—Figure 4D and Eq. 7 show that the shape of the isolines in the DBL determines exchange area as well as the direction of net diffusion. It would therefore be obvious to base calculations of horizontal influence directly on chemical measurements rather than estimating from sediment topography as proposed in this paper. Heterogeneity in oxygen uptake of sediments should cause the oxygen isolines to cross even a perfectly flat surface at angles that are not predictable from the topography. Yet the appearance of all previously published isoline data indicates that mathematically smoothed topography data will in most cases generate a virtual sediment surface that is nearly parallel to the isolines. The feasibility is further supported by the good agreement between the independent calculations based on topography and on isolines for the data of Jørgensen and Des Marais (1990).
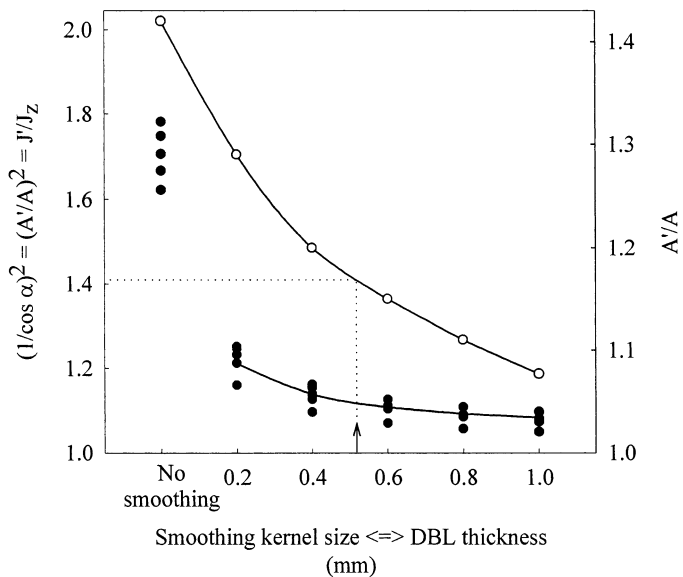
Fig. 7. Estimated ratio between total three-dimensional diffusive O_2 flux and one-dimensional vertical diffusive O_2 flux, calculated from topography with different degrees of smoothing. Filled circles originate from this study. Open circles are derived by smoothing the 3.4×3.8 mm of microbial mat surface mapped by Jørgensen and Des Marais (1990). The dotted line relates the mean Z_δ of 0.52 mm that was measured by Jørgensen and Des Marais (1990) to a correction factor slightly above 1.4. The estimates based on no smoothing correspond to isolines that strictly follow the measured topography.

If strong local hotspots of flux have a scale comparable to that of the DBL, such heterogeneity will bend the isolines sufficiently to cause significant horizontal gradients in the DBL in addition to gradients caused by surface topography. Since the relation between α and J'/J_z is not linear, the combination of topography and flux hotspots may produce effects even larger than expected from independent measurements of both phenomena. The method presented here should, therefore, be used with caution in environments where extreme heterogeneity can be expected. Examples are bioturbated, photosynthetically active, communities, where reduced sediment can be exposed on the sediment surface in direct contact with diatoms and cyanobacteria performing oxygenic photosynthesis (Fenchel 1996).

Applications of the $(1/\cos\alpha)^2$ *parameter*—Sediment and DBL topography cause one-dimensional measurements to underestimate the diffusive flux. Still, one-dimensional microprofile measurements are widely used for investigations of sediment communities. From topography-derived $(1/\cos\alpha)^2$, we are able to estimate the topography-related error caused by the one-dimensional assumption. Furthermore, $(1/\cos\alpha)^2$ provides an index of the smoothness of a sediment with respect to diffusive solute exchange across the DBL. A value of one signifies a sediment that is perfectly flat with respect to diffusive flux, while higher values indicate the influence of topography. The index is independent of the spatial resolution of the topographic data due to the well-defined smoothing procedure involved, given that the reso-

lution is high enough to resolve features of a size similar to the thickness of the DBL.

The sediment studied had been maintained in the laboratory for 2 yr, and only few parameters were thereby representative for the original sampling site. But with respect to microbial respiration and biogenic sculpturing, the system was comparable to typical fine-grained coastal sediments. The following general conclusions about constraints on the magnitude of J'/J_z are therefore valid, even though the exact values should not be extrapolated to any given marine location.

As seen in Fig. 2, the sediment surface was far from being a flat plate, and the moderate effects of topography on the flux may appear surprising. By examining the constraints on $1/\cos\alpha$, however, one realizes that even distinct topography does not necessarily create a large topographical influence on the diffusive flux: The relation between the slope of the isolines and J'/J_z is not linear. This can be realized directly from Eq. 2. As the two partial fluxes are squared before adding, the larger one will dominate the result if the difference is large. For instance, in the example in Fig. 4, the ratio J_n/J_z is only 1.14, even though the J_x is more than 50% of J_z. The fecal mounds that shaped the topography formed small islands where local horizontal fluxes were significant, superposed on a much larger background of flat surface for which J'/J_z was practically one. Even if the fecal mounds had been spaced more closely, the correction would still have been negligible on the tops and in the bottom of the valleys. Additionally, the DBL smoothes the topographic structures such that peaks are flattened and depressions filled in. Only steep features of a size easily visible induce significant topographic effects in the DBL. In conclusion, even though a sediment surface is structured into elaborate landscapes, diffusion through the DBL may still be sufficiently well modeled based on one-dimensional microprofiles and a flat plate assumption.

References

BLACKBURN, T. H., N. D. BLACKBURN, K. JENSEN, AND N. RIS-GAARD-PETERSEN. 1994. Simulation-model of the coupling between nitrification and denitrification in a fresh-water sediment. Appl. Environ. Microbiol. **60:** 3089–3095.

BOUDREAU, B. P. 1988. Mass-transport constrains on the growth of discoidal ferromanganese nodules. Am. J. Sci. **288:** 777–797.

———. 2001. Solute transport above the sediment-water interface, p. 104–126. *In* B. P. Boudreau and B. B. Jørgensen [eds.], The benthic boundary layer: Transport processes and biogeochemistry. Oxford Univ. Press.

———, AND N. L. GUINASSO. 1982. The influence of a diffusive sublayer on accretion, dissolution, and diagenesis at the sea floor, p. 115–145. *In* K. A. Fanning and F. T. Manheim [eds.], The dynamic environment at the ocean floor. Lexington.

———, AND B. B. JØRGENSEN, EDS. 2001. The benthic boundary layer: Transport processes and biogeochemistry. Oxford Univ. Press.

BRIGGS, K. B. 1989. Microtopographical roughness of shallow-water continental shelves. IEEE J. Ocean. Eng. **14:** 360–367.

CAI, W. J., AND F. L. SAYLES. 1996. Oxygen penetration depths and fluxes in marine sediments. Mar. Chem. **52:** 123–131.

CANFIELD, D. E., AND A. TESKE. 1996. Late proterozoic rise in

atmospheric oxygen concentration inferred from phylogenetic and sulphur-isotope studies. Nature **382:** 127–132.

DE BEER, D., AND P. STOODLEY. 1995. Relation between the structure of an aerobic biofilm and transport phenomena. Water Sci. Technol. **32:** 11–18.

———, ———, AND Z. LEWANDOWSKI. 1996. Liquid flow and mass transport in heterogeneous biofilms. Water Res. **30:** 2761–2765.

———, ———, F. ROE, AND Z. LEWANDOWSKI. 1994. Effects of biofilm structure on oxygen distribution and mass transport. Biotechnol. Bioeng. **43:** 1131–1138.

DENNY, M. W. 1993. Air and water. Princeton Univ. Press.

FENCHEL, T. 1996. Worm burrows and oxic microniches in marine sediments. I. Spatial and temporal scales. Mar. Biol. **127:** 289–295.

———, AND C. BERNARD. 1995. Mats of colourless sulphur bacteria. I. Major microbial processes. Mar. Ecol. Prog. Ser. **128:** 161–170.

GLUD, R. N., J. K. GUNDERSEN, N. P. REVSBECH, AND B. B. JØRGENSEN. 1994. Effects on the benthic diffusive boundary layer imposed by microelectrodes. Limnol. Oceanogr. **39:** 462–467.

———, N. B. RAMSING, J. K. GUNDERSEN, AND I. KLIMANT. 1996. Planar optrodes—a new tool for fine scale measurements of two-dimensional O_2 distribution in benthic communities. Mar. Ecol. Prog. Ser. **140:** 217–226.

GUNDERSEN, J. K., AND B. B. JØRGENSEN. 1990. Microstructure of diffusive boundary layers and the oxygen uptake of the sea floor. Nature **345:** 604–607.

GÜSS, S. 1998. Oxygen uptake at the sediment-water interface simultaneously measured using a flux chamber method and microelectrodes—must a diffusive boundary layer exist? Estuar. Coast. Shelf Sci. **46:** 143–156.

JØRGENSEN, B. B. 2001. Life in the diffusive boundary layer, p. 348–373. *In* B. P. Boudreau and B. B. Jørgenesen [eds.], The benthic boundary layer: Transport processes and biogeochemistry. Oxford Univ. Press.

———, AND D. J. DES MARAIS. 1990. The diffusive boundary layer of sediments: Oxygen microgradients over a microbial mat. Limnol. Oceanogr. **35:** 1343–1355.

———, AND N. P. REVSBECH. 1983. Colorless sulfur bacteria, Beggiatoa spp and Thiovulum spp in O_2 and H_2S microgradients. Appl. Environ. Microbiol. **45:** 1261–1270.

———, AND ———. 1985. Diffusive boundary layers and the oxygen uptake of sediments and detritus. Limnol. Oceanogr. **30:** 111–122.

KLUTE, A., AND C. DIRKSEN. 1986. Hydraulic conductivity and diffusivity: Laboratory methods, p. 687–734. *In* A. Klute [ed.], Methods of soil analysis—part 1—physical and mineralogical methods. American Society of Agronomy.

LORENZEN, J., R. N. GLUD, AND N. P. REVSBECH. 1995. Impact of microsensor-caused changes in diffusive boundary layer thickness on O_2 profiles and photosynthetic rates in benthic communities of microorganisms. Mar. Ecol. Prog. Ser. **19:** 237–241.

PAUL, A. Z., E. M. THORNDIKE, L. G. SULLIVAN, B. C. HEEZEN, AND R. D. GERARD. 1978. Observations of the deep-sea floor from 202 days of time-lapse photography. Nature **272:** 812–814.

RAFFEL, M., C. WILLERT, AND J. KOMPENHANS. 1998. Particle image velocimetry. Springer.

RASMUSSEN, H., AND B. B. JØRGENSEN. 1992. Microelectrode studies of seasonal oxygen uptake in a costal sediment: Role of molecular diffusion. Mar. Ecol. Prog. Ser. **81:** 289–303.

REVSBECH, N. P. 1989. An oxygen microsensor with a guard cathode. Limnol. Oceanogr. **34:** 474–478.

———, B. B. JØRGENSEN, AND T. H. BLACKBURN. 1979. Oxygen in the sea bottom measured with a microelectrode. Science **207:** 1355–1356.

STEINBERGER, N., AND M. HONDZO. 1999. Diffusional mass transfer at sediment-water interface. J. Environ. Eng. **125:** 192–200.

SWIFT, S. A., C. D. HOLLISTER AND R. S. CHANDLER. 1985. Close-up stereo photographs of abyssal bedforms on the Nova Scotian continental rise. Mar. Geol. **66:** 303–322.

WEISSBURG, M. J., AND R. K. ZIMMER-FAUST. 1994. Odor plumes and how blue crabs use them in finding prey. J. Exp. Biol. **197:** 349–375.

WHEATCROFT, R. A. 1994. Temporal variation in bed configuration and one-dimensional bottom roughness at the mid-shelf stress site. Cont. Shelf Res. **14:** 1167–1190.

ZIEBIS, W., S. FORSTER, M. HUETTEL, AND B. B. JØRGENSEN. 1996*a*. Complex burrows of the mud shrimp Callianassa truncata and their geochemical impact in the sea-bed. Nature **382:** 619–622.

———, M. HUETTEL, AND S. FORSTER. 1996*b*. Impact of biogenic sediment topography on oxygen fluxes in permeable seabeds. Mar. Ecol. Prog. Ser. **140:** 227–237.